EDGEWOOD CHEMICAL BIOLOGICAL CENTER
U.S. ARMY RESEARCH, DEVELOPMENT AND ENGINEERING COMMAND
Aberdeen Proving Ground, MD 21010-5424

ECBC-TR-932

REGRESSION MODEL FOR MODTRAN WITH APPLICATIONS TO INACTIVATION OF MICROBES SUSPENDED IN THE ATMOSPHERE BY SOLAR ULTRAVIOLET RADIATION

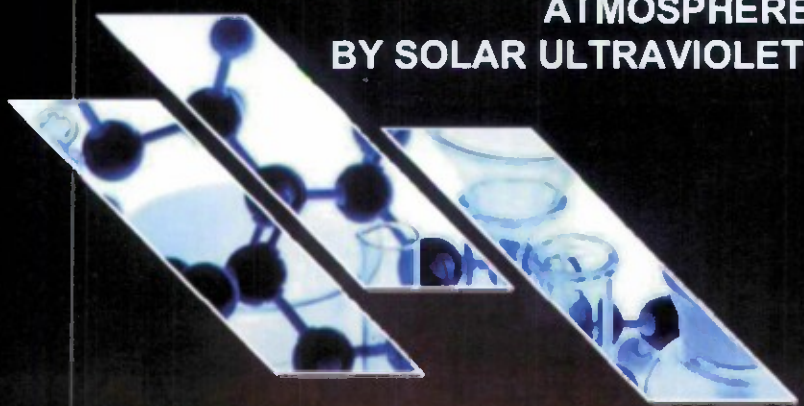

Avishai Ben-David
Jose-Luis Sagripanti

RESEARCH AND TECHNOLOGY DIRECTORATE

May 2012

U.S. ARMY RDECOM

Disclaimer

The findings in this report are not to be construed as an official Department of the Army position unless so designated by other authorizing documents.

REPORT DOCUMENTATION PAGE

Form Approved
OMB No. 0704-0188

1. REPORT DATE *(DD-MM-YYYY)*	2. REPORT TYPE	3. DATES COVERED *(From - To)*
XX-05-2012	Final	Jan 2008 - Mar 2011

4. TITLE AND SUBTITLE
Regression Model for MODTRAN with Applications to Inactivation of Microbes Suspended in the Atmosphere by Solar Ultraviolet Radiation

5a. CONTRACT NUMBER

5b. GRANT NUMBER

5c. PROGRAM ELEMENT NUMBER

6. AUTHOR(S)
Ben-David, Avishai; and Sagripanti, Jose-Luis

5d. PROJECT NUMBER

5e. TASK NUMBER

5f. WORK UNIT NUMBER

7. PERFORMING ORGANIZATION NAME(S) AND ADDRESS(ES)
DIR, ECBC, ATTN: RDCB-DRD-P, APG, MD 21010-5424

8. PERFORMING ORGANIZATION REPORT NUMBER
ECBC-TR-932

9. SPONSORING / MONITORING AGENCY NAME(S) AND ADDRESS(ES)
U.S. Army Edgewood Chemical Biological Center, Aberdeen Proving Ground, MD 21010-5424

10. SPONSOR/MONITOR'S ACRONYM(S)
ECBC

11. SPONSOR/MONITOR'S REPORT NUMBER(S)

12. DISTRIBUTION / AVAILABILITY STATEMENT
Approved for public release; distribution is unlimited.

13. SUPPLEMENTARY NOTES
This work was funded by an In-House Laboratory Independent Research grant from ECBC.

14. ABSTRACT-LIMIT 200 WORDS
The inactivation of airborne viral pathogens by solar radiation is relevant to public health and biodefense. We developed a simple nonlinear least-squares regression model for a wide variety of MODerate resolution atmospheric TRANsmission (MODTRAN) derived quantities that are useful for theoretical and experimental work in microbicidal UV radiation studies (280–320 nm) where the survival time of viruses in the atmosphere is determined. The virus action spectrum (inactivation sensitivity in UV wavelengths) used in the regression model represents a diverse range of viruses. In this report, we outline in detail the procedure of computing the regression coefficients. To our knowledge, this is the first time that a comprehensive regression model has been attempted successfully for a complex radiative transfer scenario in the atmosphere as a function of altitude, ground albedo, and sea-level visibility distance. The regression model enables the predictions of the maximum number of radiation-days a virus will survive in the atmosphere under clear skies at a given altitude above a surface with given albedo and visibility conditions. The excellent agreement between the regression model data and MODTRAN computations should encourage other researchers to seek simple regression models to complement the more laborious MODTRAN computations in a variety of applications.

15. SUBJECT TERMS
Radiative transfer; Multiple scattering; Regression model; MODTRAN; Photobiology; Virus inactivation; Microbicidal UV radiation

16. SECURITY CLASSIFICATION OF:			17. LIMITATION OF ABSTRACT	18. NUMBER OF PAGES	19a. NAME OF RESPONSIBLE PERSON
a. REPORT	b. ABSTRACT	c. THIS PAGE			Renu B. Rastogi
U				6	19b. TELEPHONE NUMBER *(include area code)* (410) 436-7545

Blank

PREFACE

The work described in this report was authorized under the In-House Laboratory Independent Research grant from the U.S. Army Edgewood Chemical Biological Center. This work was started in January 2008 and completed in March 2011.

The use of either trade or manufacturers' names in this report does not constitute an official endorsement of any commercial products. This report may not be cited for purposes of advertisement.

This report has been approved for public release.

Blank

CONTENTS

FIGURE

TABLES

REGRESSION MODEL FOR MODTRAN WITH APPLICATIONS TO INACTIVATION OF MICROBES SUSPENDED IN THE ATMOSPHERE BY SOLAR ULTRAVIOLET RADIATION

1. INTRODUCTION

The inactivation of airborne viral pathogens is relevant to public health and biodefense. In a recent paper (*1*), we described MODerate resolution atmospheric TRANsmission (MODTRAN), a software program developed by Spectral Sciences, Inc. (Burlington, MA) and the U.S. Air Force Research Laboratory (Wright-Patterson Air Force Base, OH) (*2*). Using MODTRAN, we explored the effects of altitude, sea-level meteorological visibility distance, and surface (ground) albedo on the inactivation of viruses due to direct and diffuse solar UV in the wavelength range 280–320 nm (known as UVB) in a clear-sky atmosphere (*3*).

Virucidal solar radiation consists of a direct solar UV and a diffuse UV component, which is produced by the multiple scattering of light by ambient atmospheric aerosols and gases and the multiple reflections of UV by the underlying surface or ground. In this study, we extend the regression model results, which were limited to diffuse and total irradiances in our previous work (*1*), and we outline the general procedure to compute the regression coefficients. The procedure may be useful for setting other MODTRAN irradiance computations in the framework of a simple-to-use regression model.

In our previous paper (*1*), we discussed the difference between plane (horizontal) irradiances and spherical (actinic) fluxes (horizontal irradiances are smaller than actinic fluxes), and their effect on predicting the number of days a spherical virus can survive in the atmosphere. In this study, we compute the regression model only for MODTRAN plane-irradiances. Our regression model assumes the specific shape of an action spectrum that is responsible for the inactivation of the viruses.

MODTRAN is a numerical code that is accepted by the scientific community, and it is commonly used to address diffuse sky radiance, multiple scattering, and band-models gas absorption. MODTRAN has been extensively verified and validated (*4*). The main drawbacks of MODTRAN are its complexity (the user must be an expert in MODTRAN to be able to use it correctly) and its application is time consuming (many MODTRAN runs are needed to compute UV daily energy). In addition (true for any numerical code), the output of each run from MODTRAN is numbers; thus, intuitive insight for the effect of key parameters on the output is lost. To overcome MODTRAN complexity, we use a simple nonlinear regression model that gives the user the functional dependence of UV on key environmental parameters (altitude, albedo, and visibility).

The importance of a regression model for MODTRAN results cannot be overstated. The size of MODTRAN data used to compile the regression model (Tables 1–5) is ~2 GB (only for MODTRAN *flx* and *tp5* data files), and it takes hours of central processing unit (CPU) time (on a fast personal computer). We acknowledge that with greater expertise of

MODTRAN execution, data storage and CPU time may be optimized. We also acknowledge that there are many available products (*5*)* that ease the complexity of operating MODTRAN and may reduce CPU time, but the regression model proposed here is virtually instantaneous.

The novelty and usefulness of our comprehensive regression model is that it can "replace" MODTRAN for this particular problem (inactivation of microbes suspended in the atmosphere by solar UV radiation) without reducing accuracy significantly. This approach contrasts previous studies where MODTRAN output for specific limited parameters (e.g., UV transmission [*6*], water temperature retrieval [*7*], and radiance along a specific flight line [*8*]) were fitted with a regression model. These types of regression fits, while being useful, were not substitutes for the MODTRAN vast complex output that our regression model was able to capture. Our goals are to demonstrate that a comprehensive regression model is feasible (for the limited UVB wavelength range in our germicidal application), to give details of how to develop it, and to encourage others to attempt this course of action for other MODTRAN applications.

This report is organized as follows. In Section 2, we briefly present the terminology and geometry of the radiative transfer for virus inactivation in the presence of UV radiation in a MODTRAN atmosphere. In Section 3, we outline a simple-to-use nonlinear least-squares regression model for UV radiation fields, such as total daily energy, maximum ambient flux at noon, and various ratios of energy to flux, that are key components for estimating virus inactivation in theoretical and experimental studies. In Section 3.1, we explore the range of the environmental parameters (altitude, ground albedo, and sea-level visibility distance) for the regression model, and in Section 3.2, we give details on how to compute the regression model coefficients from MODTRAN simulated atmospheres. In Section 4, we compare the results obtained with the regression model with MODTRAN simulations . In Section 4.1, we demonstrate that the radiation fields can be adequately described with a second order regression model. Section 4.1 also provides a regression model for several atmospheres for a 35° latitude and equinox and solstice dates in the form of relatively simple tables and equations that provide a means for a quick estimate of UV radiation fields and inactivation time. In Section 4.2, we attempt the scaling of various radiation fields to different geographic locations (latitude) and dates (day of the year) to enable the use of the regression model in any given location and time of the year. We conclude with a summary in Section 5.

2. RADIATIVE TRANSFER MODEL

The radiative transfer model provides a measure of energy conservation for the input solar UV (at the top of the atmosphere). The atmosphere transforms the input solar photons into one of the following types of photons:

- Scattered photons (reflection of photons by the ground is technically considered scattering)
- Absorption photons

---

* Products such as the Electro-Optical Systems Atmospheric Effects Library (EOSAEL) and Ultraviolet Transmission and Lidar Simulation Model (UVTRAN).

- Emission photons (emission is usually negligible in UV wavelengths)

The optical properties of the atmosphere are vertically distributed by the following methods:

- Molecular scattering by trace gases (Rayleigh scattering [*9*])
- MIE scattering (*9*) by particulates (aerosols)
- Absorption by molecules and aerosol particles

Scattering is not restricted to one interaction (i.e., a single-scattering event) between a photon and a single molecule (or particle). A photon may be rescattered many times (multiple scattering, namely diffuse light) by molecules and aerosols. Aerosol scattering is a directional angular scattering where the angular distribution of the scattering is a complicated function of the chemical composition, size, and shape of the aerosols. The molecular absorption for infinitesimal monochromatic radiation is described by the Beer-Lambert law (*9*) and by a band model (*2*) for radiation with a given spectral width. To complicate matters further, some of the scattered photons are reflected by the underlying surface (ground), some of which undergo further scattering. In our model, we assumed spectrally uniform ground reflectance for convenience.

We divided MODTRAN parameters into spatial and temporal parameters. Spatial parameters affect the composition of the atmosphere and temporal parameters affect the time dependence of UV radiation, and thus, they are important for computing the daily UV energy incident on a virus (i.e., integration of flux [irradiance] over time) where the solar UV zenith angle varies as a function of time. Spatial parameters are determined as $\psi = \psi(atmospheric\ optical\ properties)$,and a temporal parameter is set at θ, which is the solar zenith angle as the function of the day of year, time of day, and geographical latitude and longitude (in this work, longitude is zero); $\theta = 0$ is the zenith angle at local noon.

The notations and the geometry of the MODTRAN atmosphere were summarized in our previous paper (*1*), and they can also be found in detail in the MODTRAN user guide (*10*). The objective of the present study was to compute the radiation field at altitude h (above the ground) in the atmosphere. The spectral flux, $F(W/m^2/nm)$, per wavelength interval v at altitude h is the sum of the attenuated direct flux from the sun, upward diffuse flux, and downward diffuse flux. All fluxes at altitude h are a function of the zenith solar angle θ and the optical properties of the atmosphere ψ. We stress that both upward and downward diffuse fluxes (identified in the equations with up [$^{\uparrow}$] and down [$^{\downarrow}$] arrows) are affected by the ground albedo due to multiple scattering and reflections off the ground. All the fluxes (irradiances) considered in this paper are plane (horizontal) irradiances (i.e., irradiances that cross a horizontal unit surface).

A virus at altitude h above the ground is illuminated by two types of radiations:

- Direct (unscattered) solar UV flux attenuated by the atmosphere along the direction θ to the virus location

- Diffuse flux due to the complex interaction between the solar UV radiation, the atmosphere, and the ground

The total flux in the atmosphere is shown by

$$F^T(h,\theta,\psi,\nu) = F^{dif}(h,\theta,\psi,\nu) + F^{dir}(h,\theta,\psi,\nu) \quad (1)$$

where superscript T stands for total, *dif* for diffuse, and *dir* for direct. The directional upward and downward fluxes at altitude h were combined to one diffuse flux: $F^{dif}(h,\theta,\psi,\nu) = F_{\downarrow}^{dif}(h,\theta,\psi,\nu) + F_{\uparrow}^{dif}(h,\theta,\psi,\nu)$. The portion of the solar UV spectrum efficient in inactivating viruses lies within 280–320 nm and it is generally known as "action spectrum" (*11*, *12*). We computed two types of spectrally integrated fluxes (eq 2): Atmospheric ambient flux $F^x(h,\theta,\psi)\,(W/m^2)$ and Action flux $F_a^x(h,\theta,\psi)\,(W/m^2)$ (this flux is responsible for the inactivation of the virus). The subscript a represents action and the superscript x is reserved for total, diffuse and direct radiation. The total, diffuse and direct spectrally integrated fluxes are shown by

$$\left\{\begin{array}{l} F^x(h,\theta,\psi) = \int_{280nm}^{320nm} F^x(h,\theta,\psi,\nu)d\nu \\ F_a^x(h,\theta,\psi) = \int_{280nm}^{320nm} F^x(h,\theta,\psi,\nu)\phi_a(\nu)d\nu \end{array}\right\} \quad (2)$$

where $\phi_a(\nu)$ is an action spectrum (*1*)* that gives the spectral flux fraction (i.e., a transmission function) needed for virus inactivation. This action spectrum is believed to represent the inactivation sensitivity of diverse viruses belonging to viral families whose members cause severe diseases (*11*).

The action spectrum used in this work represents viral survival at various wavelengths with respect to the survival measured after exposure to 254 nm UV radiation (peak of DNA absorption and viral damage). Microbial sensitivity is generally expressed by the D_{37} survival rate, which corresponds to the irradiance needed to produce, on average, an inactivating hit per virion, which corresponds to a decrease of the measured survival to 37% of the viral amount originally irradiated. Although the action spectrum was built using D_{37} values measured at various wavelengths, other survival levels (*1*) can also be employed (e.g., the survival levels for 1 $\log^{10}$ or 2 $\log^{10}$ are 10% and 1%, respectively). Our regression model assumes this specific spectral shape of the action spectrum; a different spectral shape (e.g., for a different virus) will result in different numerical values for the regression model coefficients and will affect the accuracy of the regression model. The virucidal action spectrum was determined with data from many different viruses, where the target is the nucleic acid, and thus, it is unlikely that a virus will show a different action spectrum than the one we use.

We were interested in estimating the daily UV energy (a full day exposure) that a virus would experience at a specific location, even though the virus may not have maintained the same location from sunrise to sunset because of wind, turbulence, and gravitational settling. For

* An action spectrum is illustrated in Figure 3 of reference (*1*).

computing the UV inactivating daily energy, we needed to track the solar angle as a function of time. For each point in time, a new set of atmospheric fluxes was computed (eq 2). The solar zenith angle $\theta = \theta(latitude, day, hour)$ (*13*) as a function of latitude, day of year, and time of day, is given by

$$\left\{\begin{array}{l} \cos(\theta) = \sin(latitude)\sin(\delta) + \cos(latitude)\cos(\delta)\cos(ha) \\ \delta = 0.006918 - 0.399912\cos(\gamma) + 0.070257\sin(\gamma) - 0.006758\cos(2\gamma) + 0.000907\sin(2\gamma) - \ldots \\ \quad 0.002697\cos(3\gamma) + 0.00148\sin(3\gamma) \\ \gamma = \dfrac{2\pi(day - 1 + (hour - 12)/24}{365} \\ ha = \dfrac{\pi}{180} \times \\ \left(\dfrac{60\,hour + 229.18(75\times10^{-5} + 0.001868\cos(\gamma) - 0.032077\sin(\gamma) - 0.014615\cos(2\gamma) - 0.040849\sin(2\gamma))}{4} - 180\right) \\ daylight = \dfrac{2\times sunrise}{15} \quad ; \quad sunrise = \dfrac{180}{\pi}\left|\arccos(-\tan(latitude)\tan(\delta))\right| \end{array}\right. \tag{3}$$

where

δ is the solar declination angle (radians)
ha is the solar hour-angle (radians)
γ is the fractional year in radians
day is the day of the year (1 January is day 1)
hour is the hour in the day (0 to 24)
sunrise is the hour angle (degrees) for sunrise
daylight is the daylight time (hours) between *sunrise* and *sunset*

In eq 3, time of day is local solar time (*hour* = 12 noon; the sun is at the zenith and *hour* can be given as a fraction [e.g., *hour* = 11.5]). The sunrise and sunset times are the times for which the solar zenith angle is at the horizon (i.e., $\theta = 90^0$). The sunrise and sunset times are symmetric with respect to noon. Therefore, the length of daylight is easily computed as $(sunset - sunrise)/15 = 2\times sunrise/15$, where the constant 15 is the value converted from degrees to hours (the earth rotates at an angular speed of 15°/h). We can write the time-dependent solar angle θ as $\theta(\eta, t)$, where η denotes the geographical latitude and the day of the year, $\eta = (latitude, day\ of\ year)$, and t is the time (in hours) within the day. With these notations, the daily energy $E(J/m^2)$ at altitude h and location/day η is the integration of fluxes (eq 2) over time of day (t). This equation is given by

$$\left\{\begin{array}{l} E^{x}(h,\eta,\psi) = \int_{sunrise}^{sunset} F^{x}(h,\theta(\eta,t),\psi)dt \\ E_{a}^{x}(h,\eta,\psi) = \int_{sunrise}^{sunset} F_{a}^{x}(h,\theta(\eta,t),\psi)dt \\ \eta = \eta(latitude, day\ of\ year) \end{array}\right\} \quad (4)$$

where

$E^{x}(h,\eta,\psi)$ is the atmospheric daily energy

$E_{a}^{x}(h,\eta,\psi)$ is daily action-energy

The portion of the diffuse daily action-energy relative to the total is variable (from 85% near the ground to 53% at 5 km for U.S. 1976 standard atmosphere in spring-summer with rural aerosols on 21 March and latitude of 35° N) (*1*).* It is a function of visibility, albedo, and altitude (increasing with albedo, decreasing with visibility and altitude). Many monitoring institutions measure and report the ambient flux only at local-noon when the sun is at the highest point in the sky. These local-noon measurements correspond to the maximum magnitude of spectrally integrated ambient flux where the ambient flux attains its maximum magnitude: $F^{x} \rightarrow F_{\max}^{x}$. The maximum value of ambient flux is given by

$$F_{\max}^{x}(h,\eta,\psi) = F^{x}(h,\theta(\eta,t=noon),\psi) = \int_{280nm}^{320nm} F^{x}(h,\theta(\eta,t=noon),\psi,\nu)d\nu \quad (5)$$

3. METHOD OF SOLUTION

For predictions of virus inactivation, the theoretician who models the radiative transfer interaction and the experimentalist who measures the UV flux (or daily energy) may be interested in different quantities. The theoretician may be interested in the daily action energies, $E_{a}^{T}(h,\eta,\psi)$, $E_{a}^{dif}(h,\eta,\psi)$, and $E_{a}^{dir}(h,\eta,\psi)$, as functions of atmospheric parameters ψ and location (h,η). The experimentalist who measures the ambient atmospheric fluxes at noon may want to scale the noon-time measurements, $F_{\max}^{T}(h,\eta,\psi)$, $F_{\max}^{dif}(h,\eta,\psi)$, and $F_{\max}^{dir}(h,\eta,\psi)$, to daily action energies.

Computing daily action energies with MODTRAN is complex and time-consuming. For each time increment t and atmospheric condition ψ in eq 4 (e.g., surface albedo or meteorological visibility range), a new MODTRAN run must be made and numerical integration of the results must be performed. Our objective in this study is to develop a relatively simple regression model that reproduces MODTRAN results and eqs 2, 4, and 5 within acceptable accuracy without intensive computations. To the best of our knowledge, a regression model has not been attempted successfully on MODTRAN. However, in this study (it may be due to the spectral shape of the action spectrum and the relatively narrow wavelength range), we

* Illustrated by Figure 5 in reference (*1*).

were pleasantly surprised to see that reasonable accuracy in the regression model was accomplished (Section 4).

Our simple regression model addresses nine quantities: three daily action energies (total, diffuse, and direct) and six ratios given by

$$\left\{\begin{array}{l}
\dfrac{E_a^T(h,\eta,\psi)}{F_{\max}^T(h,\eta,\psi)}\ (\mathrm{s}) = \text{total daily action-energy normalized to total ambient flux at noon} \\
\dfrac{E_a^{dif}(h,\eta,\psi)}{F_{\max}^{dif}(h,\eta,\psi)}\ (\mathrm{s}) = \text{diffuse daily action-energy normalized to diffuse ambient flux at noon} \\
\dfrac{E_a^T(h,\eta,\psi)}{F_{\max}^{dir}(h,\eta,\psi)}\ (\mathrm{s}) = \text{total daily action-energy normalized to direct ambient flux at noon} \\
\dfrac{E_a^{dif}(h,\eta,\psi)}{E_a^T(h,\eta,\psi)} = \text{fraction of diffuse daily action-energy in total daily action-energy} \\
\dfrac{E^{dir}(h,\eta,\psi)}{E_a^T(h,\eta,\psi)} = \text{ratio of direct daily ambient energy (w/o effect of virus action spectrum)} \\
\qquad\qquad \text{to totaldaily action-energy} \\
\dfrac{F_{\max}^{dif}(h,\eta,\psi)}{F_{\max}^T(h,\eta,\psi)} = \text{fraction of ambient diffuse flux at noon in total ambient flux at noon} \\
E_a^T(h,\eta,\psi) = \text{total daily action-energy}(\mathrm{J/m^2}) \\
E_a^{dif}(h,\eta,\psi) = \text{diffuse daily action-energy}(\mathrm{J/m^2}) \\
E_a^{dir}(h,\eta,\psi) = \text{direct daily action-energy}(\mathrm{J/m^2})
\end{array}\right. \tag{6}$$

All of the quantities in eq 6, except E_a^T and E_a^{dif}, are new and were not included in our previous paper (*1*). For practical reasons (to be explained in Section 3.2), we chose to compute the inverse (reciprocal) of $\dfrac{E_a^T(h,\eta,\psi)}{F_{\max}^{dir}(h,\eta,\psi)}$ and $\dfrac{E_a^{dif}(h,\eta,\psi)}{E_a^T(h,\eta,\psi)}$ (see Section 4, Tables 1–4). Several other useful quantities can be derived from the nine quantities in eq 6. For example, the ambient atmospheric fluxes (i.e., total, direct, and diffuse ambient fluxes that illuminate the virus at altitude *h*, without the effect of the virus action spectrum) and the ambient atmospheric direct (unscattered) daily energy can be calculated by

$$\left\{\begin{array}{l}
F_{\max}^{dif}(h,\eta,\psi) = E_a^{dif}(h,\eta,\psi) \Big/ \dfrac{E_a^{dif}(h,\eta,\psi)}{F_{\max}^{dif}(h,\eta,\psi)} \\
F_{\max}^{T}(h,\eta,\psi) = E_a^{T}(h,\eta,\psi) \Big/ \dfrac{E_a^{T}(h,\eta,\psi)}{F_{\max}^{T}(h,\eta,\psi)} \\
F_{\max}^{dir}(h,\eta,\psi) = F_{\max}^{T}(h,\eta,\psi) - F_{\max}^{dif}(h,\eta,\psi) \\
E^{dir}(h,\eta,\psi) = E_a^T(h,\eta,\psi) \times \dfrac{E^{dir}(h,\eta,\psi)}{E_a^T(h,\eta,\psi)}
\end{array}\right. \tag{7}$$

With our regression model, we can retrieve 13 quantities of potential biological utility as shown by eqs 6 and 7. We caution the reader that with the regression model coefficients (given in Tables 1–4 for eq 6), eq 7 results show an amplification of errors (e.g., the relative error in a calculated ratio x/y where x and y suffer 10% error is 20% for uncorrelated errors), which lowers the accuracy obtained by eq 6.

After carefully considering the contribution of various parameters to virus irradiation in the atmosphere, three parameters were selected for the regression analysis:

- The altitude of viruses above the ground h
- The surface albedo (reflectivity) of the land underneath the airborne virsues
- The visibility range (inversely proportional to aerosol number density)

The relative humidity (RH) is also highly variable, but its effect is accounted for in MODTRAN simulations by the visibility distance parameter. We pursued a regression model in the form $y(h, alb, vis \mid \eta, \psi)$ that captured the parameter space (altitude, albedo, and visibility) for each of the nine quantities (six ratios and three daily action-energies) at a given geographic location and day of the year (η) and atmosphere (ψ).

The effect of the vertical transport of viruses due to air currents could be incorporated in the model (in principle) by computing a regression model as a function of altitude, visibility, and albedo for each hour and summing the altitude-dependent energy within time span t_1 to t_2, if the whereabouts (altitude) of the virus is known. We chose only to compute the energy within daylight (sunrise to sunset) to maintain a relatively simple approach. We note that the falling velocity of a small spherical particle in the atmosphere is very small; a particle <1 μm diameter (the size of an agglomerate of viruses is on the order of microns, the size of a single virus is in the range of 0.01 to 0.1 μm) with a density of 1 g/m^3 will fall in calm air (no air turbulence and no vertical air currents) at a terminal gravitational settling velocity of $\sim 3 \times 10^{-5}$ *m/s*. Thus, within 24 h, a particle will fall less than 3 m.

3.1 Parameter Space for Regression Model

Altitude.

We restricted the altitude h above the ground to a range of values $0 \le h \le 5\ km$. These values encompass most scenarios of interest for the potential location of viruses in the atmosphere. In the numerical grid for h, we used more values near the ground in order to capture the complexity of the radiative transfer model in the boundary layer (where most of the ambient atmospheric aerosols reside). Twenty values were chosen for h: 0, 0.005, 0.01, 0.02, 0.05, 0.075, 0.1, 0.15, 0.2, 0.3, 0.4, 0.5, 0.75, 1.5, 2, 2.5, 3, 4, and 5 km.

Sea-level visibility range.

The sea-level (surface) visibility meteorological range, *vis*, in MODTRAN is based on 1926 Koschmieder's theory (*14*), where visibility is given as a function of the surface aerosol extinction at wavelength 550 nm:

$$vis(km) = \frac{3.912}{aerosol\ \ extinction\ (km^{-1}) + 0.01159\ (km^{-1})} \tag{8}$$

where 0.01159 is the molecular scattering coefficient at 550 nm and 3.192 is log(2%) for the assumed 2% brightness contrast with which the visibility range is defined.

Equation 10 shows that the aerosol loading in the atmospheric boundary layer (i.e., surface aerosol extinction in the denominator) determines the visibility distance. In our study, we used this (MODTRAN) definition for visibility range. Later studies (*15*) revised the relationship between reported visibility ranges (by observers in meteorological stations) and an aerosol extinction coefficient to be $observed\ vis(km) = (1.9/3.912) \times vis \cong vis/2$ because visual targets used by the observer to assess visibility distance are

- Not black
- Frequently too small in angular size
- Located only at quantized distances

This modified visibility range (*15*) was used (*16*) to estimate the distribution of continental surface aerosol extinction. It was found that the extinction coefficient in the eastern United States was relatively modest (0.1–0.2 km^{-1}). The observed visibility range was 9.5–19 km, which corresponds to a MODTRAN visibility of 19–38 km.

In UV wavelengths, a RH > ~75% alters the optical properties of aerosols (such as the single-scattering albedo) and thus modifies aerosol extinction. Most of the ambient aerosols reside in the atmospheric boundary layer (0–2 km), where the effect of RH is pronounced. When the visibility distance is set in MODTRAN (eq 8) the number density of the aerosols (i.e., aerosol loading) is scaled to produce the appropriate extinction. Thus, when the RH in a MODTRAN atmosphere is modified (as an input), the effect of RH on the aerosols is mostly cancelled by rescaling the extinction (that was altered by RH) with the visibility parameter. For this reason (verified in our simulations), we chose not to have RH as a parameter in the regression model. In the regression model, we restricted MODTRAN visibility (eq 8) to the range $15\ km \le vis \le 100\ km$, which spans the observed visibility range of 7.6–69 km. Eleven values were chosen to span the visibility space: 15, 20, 25, 30, 40, 50, 60, 70, 80, 90, and 100 km.

Surface albedo.

The measured UV albedo values of most natural surfaces are smaller than 10%. The albedo (MODTRAN *surref* parameter) was assumed to be spectrally uniform between 280 and 320 nm. Several spectral albedo values (MODTRAN internal database in [*2*]) at 200 nm (and values in parentheses at 500 nm) are

- Grassland: 0.025 (0.065)
- Mixed forest (consisting of 70% broadleaf and 30% pine): 0.025 (0.036)
- Urban (commercial): 0.026 (0.036)
- Deciduous needle forest (broadleaf-pine): 0.017 (0.032)
- Closed shrubs (pine brush): 0.012 (0.049)
- Tundra: 0.032 (0.07)
- Savanna (grass-scrub): 0.019 (0.066)
- Woody savanna (soil-grass-scrub): 0.021 (0.06)
- Crop mosaic (mixed vegetation): 0.007 (0.017)

For materials tested,

- The albedo levels of old grass, dead grass, burnt grass, and maple leaf at 300 nm were 0.07,0.1, 0.02, and 0.02, respectively.

- The albedo levels for desert sand (mixture of rocks and silt sand) at 275, 300, and 325 nm were 0.12, 0.13, and 0.14, respectively.

- The albedo level for ocean water at 300 nm was 0.027.

In the UVB region (v < 315 nm), the measured albedo (*17*) was as small as 0.016–0.017 over vegetation, 0.04–0.05 over bare fertile soil, and 0.07–0.10 over concrete (autobahn, Germany). The albedo over dry bright sand (e.g., ocean beach) was 0.14 at 300 nm.

3.2 Second Order Regression Model

In this section, we give details of how to compute the regression model from MODTRAN results to enable the reader to construct regression models for other atmospheric conditions and radiative transfer scenarios. We experimented with different options for a regression model, such as a different polynomial order with each variable (h,alb,vis), to optimize the regression model fit to the simulated data (MODTRAN output) for a given atmospheric model (η,ψ). We searched for the lowest order polynomial that showed reasonable results and ensured numerical stability of the regression model. In the regression model, we treated each variable independently and did not allow interaction (cross-terms) between variables (e.g., $h \times alb$ or $vis \times alb$) to preserve physical meaning as much as possible. We finally chose a second order polynomial $y(h,alb,vis)$ with seven coefficients, w_1 to w_7 (determined with least-squares fit to MODTRAN data), for given atmospheric conditions (η,ψ) by

$$y(h,alb,vis \mid \eta,\psi) = w_1 + w_2 h + w_3 h^2 + w_4 alb + w_5 alb^2 + w_6 vis + w_7 vis^2 \qquad (9)$$

where h is altitude in kilometers, *visibility* is in kilometers, and the *albedo* is a fraction (e.g., 10% reflectivity is an albedo of 0.1). We used eq 9 for each of the nine quantities listed in eq 6. However (for reasons of numerical stability, discussed below), we chose to do a regression model $y(h,alb,vis)$ for the inverse of $E_a^T / F_{\max}^{dir}$ and E_a^{dif} / E_a^T. These two quantities are easily retrieved by $\frac{E_a^T(h,\eta,\psi)}{F_{\max}^{dir}(h,\eta,\psi)} = \frac{1}{y(h,alb,vis)}$ and $\frac{E_a^{dif}(h,\eta,\psi)}{E_a^T(h,\eta,\psi)} = \frac{1}{y(h,alb,vis)}$. The other seven quantities (four ratios and three daily action-energies) are shown directly with the regression models $\frac{E_a^T(h,\eta,\psi)}{F_{\max}^T(h,\eta,\psi)} = y(h,alb,vis \mid \eta,\psi)$ and $E_a^T(h,\eta,\psi) = y(h,alb,vis \mid \eta,\psi)$. Assuming that the energy needed to inactivate virus X to a given survival level is E_1 (J/m^2) (*1*, *11*), using our regression model, we can estimate the maximum number of radiation-days, n_{days}, needed for inactivating virus X at altitude h in a given atmospheric model, visibility condition, and ground albedo by

$$n_{days}(h,alb,vis) = \frac{E_1}{y(h,alb,vis)} = \frac{E_1}{w_1 + w_2 h + w_3 h^2 + w_4 alb + w_5 alb^2 + w_6 vis + w_7 vis^2} \qquad (10)$$

where $y(h,alb,vis)$ refers to any of the last three quantities in eq 8. Equation 10 provides the maximum number of radiation-days because the plane irradiances underestimate the true spherical irradiances (see [*1*] for a discussion on the difference between plane and spherical fluxes). The complexity of the effects of altitude, albedo, and visibility on inactivation time was previously demonstrated and discussed (*1*)*, where the number of radiation-days needed for inactivation is 1 to 2 radiation-days in winter (at latitude 35° N, on 21 December).

To solve eq 10 for the seven coefficients, we constructed the matrix equation $\mathbf{Y} = \mathbf{A}\,\mathbf{w}$, where $\mathbf{Y}$ is a vector constructed from MODTRAN output $y(h,alb,vis \mid \eta,\psi) = (MODTRAN\ results)$ for all (1760) combinations (h,alb,vis), $\boldsymbol{A}$ is a matrix, and $\boldsymbol{w}$ is a vector of the unknown seven regression coefficients. The matrix $\boldsymbol{A}$ and vectors $\boldsymbol{Y}$ and $\boldsymbol{w}$ are shown by eq 11.

* Illustrated by Figure 6 in reference (*1*).

$$
\mathbf{A} = \begin{bmatrix}
1 & h_1 & h_1^2 & alb_1 & alb_1^2 & vis_1 & vis_1^2 \\
\vdots & \vdots & \vdots & alb_1 & alb_1^2 & vis_1 & vis_1^2 \\
1 & h_{\max} & h_{\max}^2 & alb_1 & alb_1^2 & vis_1 & vis_1^2 \\
 & & & & & & \\
1 & h_1 & h_1^2 & alb_2 & alb_2^2 & vis_1 & vis_1^2 \\
\vdots & \vdots & \vdots & alb_2 & alb_2^2 & vis_1 & vis_1^2 \\
1 & h_{\max} & h_{\max}^2 & alb_2 & alb_2^2 & vis_1 & vis_1^2 \\
\vdots & \vdots & \vdots & \vdots & \vdots & \vdots & \vdots \\
1 & h_1 & h_1^2 & alb_{\max} & alb_{\max}^2 & vis_1 & vis_1^2 \\
\vdots & \vdots & \vdots & alb_{\max} & alb_{\max}^2 & vis_1 & vis_1^2 \\
1 & h_{\max} & h_{\max}^2 & alb_{\max} & alb_{\max}^2 & vis_1 & vis_1^2 \\
 & & & & & & \\
1 & h_1 & h_1^2 & alb_1 & alb_1^2 & vis_2 & vis_2^2 \\
\vdots & \vdots & \vdots & alb_1 & alb_1^2 & vis_2 & vis_2^2 \\
1 & h_{\max} & h_{\max}^2 & alb_1 & alb_1^2 & vis_2 & vis_2^2 \\
 & & & & & & \\
1 & h_1 & h_1^2 & alb_2 & alb_2^2 & vis_2 & vis_2^2 \\
\vdots & \vdots & \vdots & alb_2 & alb_2^2 & vis_2 & vis_2^2 \\
1 & h_{\max} & h_{\max}^2 & alb_2 & alb_2^2 & vis_2 & vis_2^2 \\
\vdots & \vdots & \vdots & \vdots & \vdots & \vdots & \vdots \\
1 & h_1 & h_1^2 & alb_{\max} & alb_{\max}^2 & vis_2 & vis_2^2 \\
\vdots & \vdots & \vdots & alb_{\max} & alb_{\max}^2 & vis_2 & vis_2^2 \\
1 & h_{\max} & h_{\max}^2 & alb_{\max} & alb_{\max}^2 & vis_2 & vis_2^2 \\
\vdots & \vdots & \vdots & \vdots & \vdots & \vdots & \vdots \\
\vdots & \vdots & \vdots & \vdots & \vdots & \vdots & \vdots \\
1 & h_1 & h_1^2 & alb_{\max} & alb_{\max}^2 & vis_{\max} & vis_{\max}^2 \\
\vdots & \vdots & \vdots & alb_{\max} & alb_{\max}^2 & vis_{\max} & vis_{\max}^2 \\
1 & h_{\max} & h_{\max}^2 & alb_{\max} & alb_{\max}^2 & vis_{\max} & vis_{\max}^2
\end{bmatrix}
\quad
\mathbf{Y} = \begin{bmatrix}
y(h_1, alb_1, vis_1) \\
\vdots \\
y(h_{\max}, alb_1, vis_1) \\
 \\
y(h_1, alb_2, vis_1) \\
\vdots \\
y(h_{\max}, alb_2, vis_1) \\
 \\
\vdots \\
y(h_1, alb_{\max}, vis_1) \\
\vdots \\
y(h_{\max}, alb_{\max}, vis_1) \\
 \\
y(h_1, alb_1, vis_2) \\
\vdots \\
y(h_{\max}, alb_{\max}, vis_2) \\
\vdots \\
\vdots \\
y(h_1, alb_{\max}, vis_{\max}) \\
\vdots \\
y(h_{\max}, alb_{\max}, vis_{\max})
\end{bmatrix}
\quad
\mathbf{w} = \begin{bmatrix}
w_1 \\ w_2 \\ w_3 \\ w_4 \\ w_5 \\ w_6 \\ w_7
\end{bmatrix}
\tag{11}
$$

To solve for $\boldsymbol{w}$, we performed inverse operation

$$
\mathbf{w} = \mathbf{A}^{-1}\mathbf{Y} \tag{12}
$$

where the nonsquare matrix $\mathbf{A}^{-1}$ is computed by singular value decomposition (*18*) using seven eigenveetors and eigenvalues (because the rank of the matrix **A** is rank(A) = 7) or by a Gaussian elimination algorithm with partial pivoting. The error magnifieation (i.e., the stability of the regression model to input errors in $\boldsymbol{Y}$ in the solution $\boldsymbol{w}$) is proportional to the eondition number (ratio of the largest to the smallest eigenvalues of **A**). Due to the large dynamie range in **A** (h ranges from 0 to 5 km, albedo ranges from 0 to 0.15, and visibility ranges from 15 to 100 km), to aehieve numerical stability, we normalized the variables, $h \rightarrow \frac{h}{h_{\max}}$, $alb \rightarrow \frac{alb}{alb_{\max}}$, and $vis \rightarrow \frac{h}{vis_{\max}}$, in the matrix **A**. As a result of the normalization, we had to rescale the solution $\mathbf{w} = \mathbf{A}^{-1}\mathbf{Y}$ so that

$w_2 \to \frac{w_2}{h_{\max}}$; $w_3 \to \frac{w_3}{h_{\max}^2}$; $w_4 \to \frac{w_4}{alb_{\max}}$; $w_5 \to \frac{w_5}{alb_{\max}^2}$; $w_6 \to \frac{w_6}{vis_{\max}}$; $w_7 \to \frac{w_7}{vis_{\max}^2}$ (the first coefficient w_1 remained unchanged) to obtain a stable regression model (eq 9). With this normalization procedure, the condition number improved (i.e., it decreased) from 236,410 to 33.3. The maximum error magnification equals $5.7 = \sqrt{33}$ and the mean relative-error magnification (*19*) was $\frac{|\delta \mathbf{w}|/|\mathbf{w}|}{|\delta \mathbf{Y}|/|\mathbf{Y}|} = \frac{\sqrt{\max\ eigenvalue / \min\ eigenvalue}}{7}$, where $\|$ denotes a vector norm, $\delta \mathbf{w}/\mathbf{w}$ is the relative error in $\boldsymbol{w}$, and $\delta \mathbf{Y}/\mathbf{Y}$ is the relative error in MODTRAN output. The mean error magnification for the seven-element vector $\boldsymbol{w}$ is $0.82 = \sqrt{33}/7$. This value is small enough to ensure stability and accuracy of the solution $\boldsymbol{w}$ for the regression model given in eq 9.

4. RESULTS

We computed a regression model (Tables 1–4) for MODTRAN atmospheres (MODTRAN parameter *model* = 2, 3, 6), which showed 1976 U.S. standard and mid-latitude atmospheres for two types of ambient aerosols. These atmospheres represented rural and urban environments (MODTRAN parameter *ihaze* was either 1 or 4; please note that MODTRAN parameter *vis* alters the concentration [number density] of aerosols in the atmospheric boundary layer, as set by *ihaze,* to comply with the desired visibility distance). For each atmosphere, we evaluated the performance of the regression model during two seasons: spring-summer and fall-winter (MODTRAN parameter *iseasn* was either 1 or 2), and four dates (equinoxes and solstices, 21 March, 21 June, 21 September, and 21 December). The concentration and altitude profiles of all the gases were set internally by MODTRAN default parameters. In the computations, we assumed a clear sky and a spectrally flat albedo. Because a large portion of the world population lives within 30 to 40° latitudes (*20*), we chose a latitude of 35° for our calculations. In section 4.2, we show our scaling (Table 5) of the regression model to other latitudes (25, 35, and 45°) and times of year (1 February, 1 May, 1 August, and 1 November).

4.1 Regression Model

Rational for a second order regression model.

The Figure supports the selection of the second order regression model described by eq 9 with altitude, albedo, and visibility as variables. The attenuation in the atmosphere is an exponential process with optical depth (e.g., Beer's law for the direct component of the solar UV) that is nonlinear with altitude, as is shown in the curvature (steeper at lower altitudes) of the direct daily action-energy (Figure c). The nonlinear effect of altitude is also evident in the curvature of the surfaces in Figure b and in the nonuniform spacing of the surfaces in Figure a (e.g., the spacing between the 1 and 3 km surfaces is larger than the spacing between 3 and 5 km). This observation led us to choose a regression model with second order polynomial with altitude, $y(h, alb, vis \mid \eta, \psi) \propto w_2 h + w_3 h^2$ in eq 9. The nonlinear effect of visibility is evident in the curvature of the surfaces in Figure a for the diffuse daily action-energy, in Figure c for the direct daily action-energy, and in Figure d for the total (diffuse + direct) daily action-energy where the

polarity of the curvature is concave near the ground and convex at higher altitude. As altitude increases, the curvature of the surfaces deereases.

The nonlinearity with respect to visibility led us to choose a regression model with the second order polynomial with visibility $y(h, alb, vis \mid \eta, \psi) \propto w_6 vis + w_7 vis^2$. The almost linear effect of albedo (linear, but with a nonzero offset) is shown in Figure a for the diffuse and in Figure d for the total. Even though the effect of albedo is nearly linear, we chose a second order polynomial with albedo $y(h, alb, vis \mid \eta, \psi) \propto w_4 alb + w_5 alb^2$ for two reasons:

(1) The ground-reflected direct flux is proportional to albedo, hence $y(h, alb, vis \mid \eta, \psi) \propto w_4 alb$.

(2) The contribution of diffuse flux due to multiple reflections off the ground is proportional to higher order effects in albedo.

At short wavelengths (e.g., a visible wavelength region where thermal emission is negligible), the diffuse flux is proportional to $alb/(1 - alb \times S)$ *(21)*, where S is the atmospheric spherical albedo (the portion of radiation that is refleeted from the atmosphere back to the ground as a result of isotropie illumination from the ground). A second order Taylor series expansion of $alb/(1 - alb \times S)$ is shown by $alb/(1 - alb \times S) \cong alb + S \times alb^2$. Thus, the seeond order polynomial with albedo, $y(h, alb, vis \mid \eta, \psi) \propto w_5 alb^2$, is due to the linear effect of the ground-reflected direct solar photons and the quadratic effect for diffuse photons.

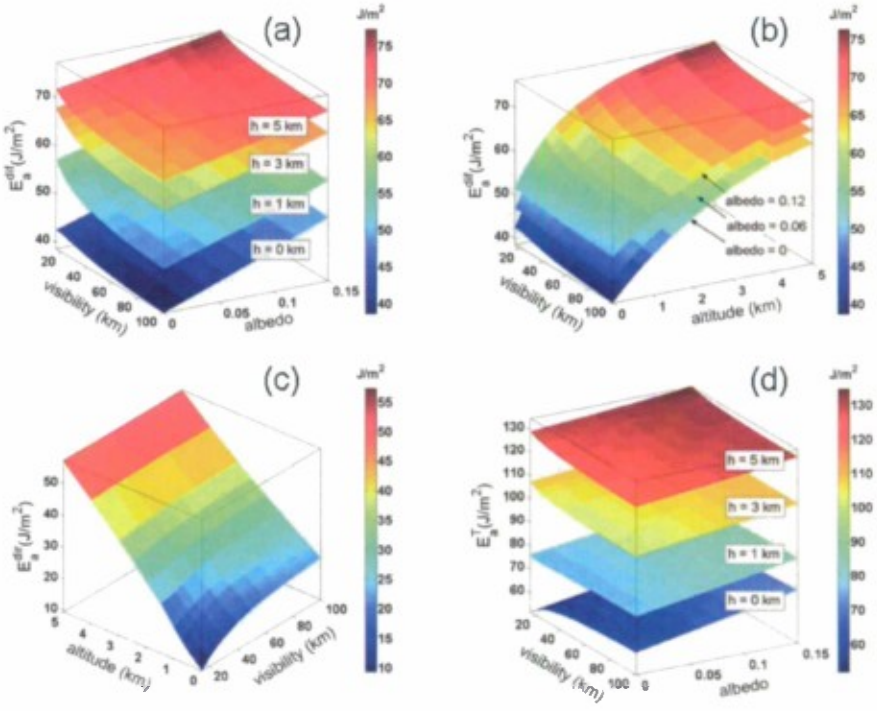

Figure. Rationale for using a second order regression model for altitude, visibility, and albedo demonstrated with 1976 U.S. standard atmospheric model, at spring-summer with rural aerosols, at latitude 35° on 21 March. **(a)** Daily diffuse action-energy $E_a^{dif}(h, albedo, visibility)$ as a function of visibility range and ground albedo for four altitudes above ground (in ascending order); 0 (bottom surface), 1, 3, and 5 km (top surface). **(b)** Daily diffuse action- energy $E_a^{dif}(h, albedo, visibility)$ as a function of altitude and visibility for three values of ground albedos; 0.12 (top surface), 0.06 (middle surface), 0 (bottom surface). **(c)** Direct action- energy $E_a^{dir}(h, visibility)$ as a function of altitude and visibility (the direct component is independent of albedo). **(d)** Daily total (diffuse + direct) action-energy $E_a^{T}(h, albedo, visibility)$ as a function of visibility range and ground albedo for four altitudes above ground (in ascending order); 0 (bottom surface), 1, 3, and 5 km (top surface).

Regression model for various atmospheres.

Tables 1–4 show the application of the regression model for 1976 U.S. standard atmosphere and for mid-latitude atmosphere, with rural and urban aerosol models at the four days of equinox and solstice at latitude 35°. For 21 March and 21 June, we used a spring-summer seasonal model, and for 21 September and 21 December, we used a fall-winter seasonal model. The season (parameter *iseasn* = 1 and 2 in MODTRAN) only affected the aerosol profile in the troposphere (2–10 km) and stratosphere (10–30 km). There are two mid-latitude atmospheric models (parameter *model* = 2 and 3 in MODTRAN); mid-latitude-summer and mid-latitude-winter. For 21 September and 21 December, we used (Tables 3 and 4) the atmospheric model mid-latitude-winter, and for 21 March and 21 June, we used the atmospheric model mid-latitude-summer. The atmospheric model set the altitude distribution of temperature,

pressure, and concentration profile of trace gases in the atmosphere (*1*).* The effect of the atmospheric model and season can be assessed by employing the regression model for different choices of atmospheric models and seasons (*1*). The regression model coefficients were computed for all nine quantities (eq 6) over all parameter spaces (h, alb, vis). The mean absolute error and the maximum absolute error are given in the tables for each of the nine quantities. The mean (average) of the absolute error is the absolute percentage difference between the regression model in eq 9 and MODTRAN output (regarded as "truth") averaged over all the parameter spaces: all altitudes ($0 \le h \le 5km$), albedos ($0 \le alb \le 0.15$), and MODTRAN visibilities ($15 \le vis \le 100km$). The maximum absolute error computed for a probability $P \ge 0.9$ gives the error for which 90% of all $y(h, alb, vis)$ regression-model values fall within MODTRAN truth values: $\max(|error|) = \int_0^{|error|} \text{Probability}(|error|)\, d(|error|) = 0.9$. Closer inspection of the coefficients in the tables reveals that because $E_a^T = E_a^{dif} + E_a^{dir}$, the regression coefficients for E_a^{dir} are (within round-off errors) the difference between the regression coefficients for E_a^T and E_a^{dif}. The tables demonstrate (see second to last columns in each of Tables 1–4) that the regression model shows a very close approximation to MODRAN results. The worst accuracy is ~6% for radiation fields E_a^{dir} and $F_{\max}^{dir} / E_a^T$ at Dec 21. For all other quantities, the error is <5%, and in most cases, it is <2%. This agreement appears excellent, especially in contrast to errors in microbiological laboratory experiments where the survival level of viruses to UV radiation is usually measured within an accuracy no better than $\pm 0.5 \log_{10}$ units ($1 \log_{10}$ is a survival level of 10%). We remind the reader that we chose to do a regression model $y(h, alb, vis)$ for the inverse (reciprocal) of $E_a^T / F_{\max}^{dir}$ and E_a^{dif} / E_a^T. Therefore, E_a^{dif} / E_a^T is shown (Table 1, 21 March) as $\frac{E_a^{dif}(h, alb, vis)}{E_a^T(h, alb, vis)} = \frac{1}{1.21 + 0.0647h + 0.00387h^2 - 0.751 alb + 0.728 alb^2 + 0.00696\ vis - 3.81 \times 10^{-5} vis^2}$ and the quantity (eq 7) $F_{\max}^T(h, alb, vis)$ is easily obtained from (Table 1, 21 March) by $F_{\max}^T(h, alb, vis) = \frac{55.7 + 17.6h - 0.923h^2 + 71.2 alb + 28.7\ alb^2 + 0.148\ vis - 0.000888 vis^2}{26.1 + 0.979h - 0.052h^2 - 1.87\ alb + 0.066\ alb^2 + 0.017\ vis - 7.08 \times 10^{-5} vis^2}$ where h and vis are in kilometers and the albedo is a fraction (0 to 1).

4.2 Location and Time Scaling of Regression Model

The regression model in Tables 1–4 was computed for a specific latitude (35°) and day of the year (equinox and solstice days). Scaling the model to other locations (latitudes) and times (dates) of interest should save enormous effort in computing new regression coefficients. Scaling the results is very challenging because the solar zenith angle, $\theta(t, latitude, day\ of\ year)$, (eq 3) varies with location and time of day. Hence, the input UV solar flux at the top of the atmosphere (the engine for all subsequent scattering) is proportional to $cos(\theta)$ and for each time of day, we have a radiative transfer model with a new input solar flux. The zenith angle also determines slant-path attenuations within the atmosphere, and the interaction with the altitude-dependent gases and aerosols is vastly different as a function of θ.

---

* See Figure 2 in reference (*1*) for the differences between the 1976 U.S. standard and mid-latitude summer and winter atmospheres.

The daily energy increases with the length of *daylight*, but because the length of daylight is linked to the solar angle, the relationship between daily-energy and length of daylight is far from simple. Nevertheless, we attempted location/time scaling and were able to produce reasonable results for six quantities: $\frac{E_o^T}{F_{\max}^T}; \frac{E_o^{dif}}{F_{\max}^{dif}}; \frac{F_{\max}^{dif}}{F_{\max}^T}; E_a^T; E_a^{dif}; E_a^{dir}$. We found a simple scaling with latitude/day as a function of solar zenith angle and length of daylight. The scaling (for any given atmospheric model) from a reference latitude and date to latitude and date is given in eq 16. The reference latitude and date were chosen to be 35° and 21 March for the given atmosphere. Although we could not establish a physical explanation, we noted that powers of cosine angle (e.g., second, third, and fourth powers, used in our scaling) are common in determining irradiance produced by a diffuse source (*22*)

$$\frac{y(h,alb,vis,latitude,day)}{y(h,alb,vis,lat=35^o,day=Mar\ 21)} = \begin{Bmatrix} \frac{\cos^2[\theta(lat,day)]}{\cos^2[\theta(35^o,Mar\ 21)]} & for \quad y = \begin{Bmatrix} \frac{E_a^T(h,alb,vis)}{F_{\max}^T(h,alb,vis)} \text{ and } \frac{E_a^{dif}(h,alb,vis)}{F_{\max}^{dif}(h,alb,vis)} \end{Bmatrix} \\ \frac{\cos[\theta(35^o,Mar\ 21)]\times daylight(lat,day)}{\cos[\theta(lat,day)]\times daylight(35^o,Mar\ 21)} & for \quad y = \frac{F_{\max}^{dif}(h,alb,vis)}{F_{\max}^T(h,alb,vis)} \\ \frac{\cos^3[\theta(lat,day)]\times daylight(lat,day)}{\cos^3[\theta(35^o,Mar\ 21)]\times daylight(35^o,Mar\ 21)} & for\ y = \begin{Bmatrix} E_a^T(h,alb,vis) \\ E_a^{dif}(h,alb,vis) \end{Bmatrix} \\ \frac{\cos^4[\theta(lat,day)]\times daylight(lat,day)}{\cos^4[\theta(35^o,Mar\ 21)]\times daylight(35^o,Mar\ 21)} & for\ y = E_a^{dir}(h,alb,vis) \end{Bmatrix} \quad (13)$$

where θ is the solar zenith angle at noon (shown in eq 3 for *hour* = 12) as a function of latitude, and *daylight* is the length of daylight in hours (eq 3). For example, the total daily action-energy for 45° latitude on 1 August for 1976 U.S. standard atmosphere with rural aerosol model at spring-summer (Table 1) is given by eq 13 as

$$E_a^T(h,alb,vis,45^o,Jun21) = 1.246\times(55.7+17.6\,h-0.923\,h^2+71.2\,alb+28.7\,alb^2+0.148\,vis-0.000888\,vis^2)$$

where the magnitude scaling constant of (1.246) $\frac{\cos^3[\theta(45^o,Aug\ 21)]\times daylight(45^o,Aug\ 21)}{\cos^3[\theta(35^o,Mar\ 21)]\times daylight(35^o,Mar\ 21)} = 1.246$

is computed from eq 3 for 21 August (233rd day of the year) at 45° latitude where $\theta = 32.63^o$ (at noon) and $daylight = 13.69\ hours$; and for the reference 21 March (80th day of the year) at 35° latitude where $\theta = 35.11^o$ (noon).

We emphasize that this is only a magnitude scaling, and it does not reshape the dependence (vertical profile) of the variable (i.e., the ratio, $\frac{y(h,alb,vis,latitude,day)}{y(h,alb,vis,lat=35^o,day=Mar\ 21)}$, is a constant that is not a function of *h*, *alb*, and *vis*). This is a deficiency in the location/time scaling, but it produces reasonable results as is evident in Table 5. In Table 5, we show the error in latitude/time scaling for 1976 U.S. standard atmosphere and mid-latitude summer atmosphere with rural and urban aerosols (noted as atmospheres A, B, C, and D) when we scale the reference atmosphere (21 March and 35° latitude) to latitudes 25, 35, and 45° for four dates (1 February, 1 May, 1 August, and 1 November). The scaling results for these six quantities are very satisfactory for some days/latitudes (<5% error), but for the other days/latitudes, the errors are as high as 50% (e.g., ~50% for E_a^{dir} and ~40% for E_a^T at February and November for 45° latitude). The average of all 288 entries in Table 5 is ~10%, whereas the error is ≤5% for 130 entries.

Thus, the simple approach of scaling to predict the solar UV irradiance received by airborne viral pathogens in the atmosphere with <50% error should be useful for theoretical studies of UV inactivation of viruses in the atmosphere, where virus survival is estimated in logarithmic scale with large uncertainty ($\pm 0.5 \log_{10}$).

5. CONCLUSIONS

Inactivation of viruses suspended in clear-sky atmosphere due to direct and diffuse solar UV was previously (*1*) calculated with MODTRAN plane irradiances. However, MODTRAN is a complex coded software program, and computing daily energies is time consuming. Therefore, we developed a simple nonlinear regression model that can produce various quantities (eqs 6 and 7) within a reasonable accuracy (~5% of the values produced by MODTRAN) that are useful to theoretical and experimental UV inactivation studies. Development of a regression model also provided an insight into the dependence of key parameters (altitude, albedo, and visibility), whereas MODTRAN (a numerical code) "only" provided numerical (though extremely accurate) output. To the best of our knowledge, this was the first time that a comprehensive regression model was demonstrated on MODTRAN atmospheric radiances. With the spectral shape of the action spectrum and the narrow wavelength range of 280–320 nm, we were pleasantly surprised that a reasonable accuracy in the regression model was accomplished for our application (Tables 1–4, last two columns).

We chose nine quantities (listed in eq 6 and shown in Tables 1–4) for the regression model (normalized by ambient radiation fields). These quantities may be useful in experimental work when one wants to rescale measured ambient data, and the absolute quantities may be useful for theoretical studies. The nine quantities were $E_a^T, E_a^{dif}, E_a^{dir}$ (total, diffuse and direct daily action-energies), $E_a^T / F_{\max}^T$, $E_a^{dif} / F_{\max}^{dif}$, $E_a^T / F_{\max}^{dir}$ (daily action-energies that are normalized by atmospheric ambient flux measured at noon), E_a^{dif} / E_a^T, E_a^{dir} / E_a^T, and $F_{\max}^{dif} / F_{\max}^T$ (fraction diffuse and direct daily action-energy, and fraction of diffuse ambient flux at noon). From these nine quantities, we derived four additional ambient quantities (eq 7): $F_{\max}^T, F_{\max}^{dif}, F_{\max}^{dir}$ (total, diffuse, and direct ambient fluxes at noon), and E^{dir} (ambient direct daily energy).

We developed a second order regression model (to capture the nonlinearity of the radiation quantities (the Figure) in the form of $y(h, alb, vis) = w_1 + w_2 h + w_3 h^2 + w_4 alb + w_5 alb^2 + w_6 vis + w_7 vis^2$ (eq 9, Tables 1–4) for the nine quantities for atmospheric models, 1976 U.S. standard and mid-latitude atmospheres for two seasons (spring-summer and fall-winter) and four dates (equinox and solstice). The regression model reproduced MODTRAN radiation quantities with acceptable accuracy (mean accuracy of ~2%); the worst accuracy was ~6% for radiation fields E_a^{dir} and $F_{\max}^{dir} / E_a^T$ on 21 December. For all other quantities, the error was <5%. This accuracy is excellent, compared to microbiological laboratory experiments where the survival level of viruses to UV radiation was measured in log-scale units, usually within an accuracy no better than ± 0.5 $\log_{10}$ units. With our simple regression model, we can compute (eq 10) the maximum number of radiation-days, n_{days}, needed for

inactivating virus X at height h in a given atmospheric model, visibility condition, and ground albedo.

The accuracy of our regression model was satisfactory (Tables 1–4), but its utility was limited to a specific latitude (35°) and day of the year (equinox and solstice dates). One solution was to recompute regression coefficients (eq 12) for the desired latitude/date, a process that was time consuming and involved a vast number of MODTRAN runs. As an alternative, we attempted to scale (see eq 13) the regression model from a reference latitude and date (chosen as 35° latitude for 21 March) to an arbitrary latitude and day of the year. We found a simple scaling as a function of zenith angle and length of daylight for the six quantities, $E_a^T / F_{\max}^T$, $E_a^{dif} / F_{\max}^{dif}$, $F_{\max}^{dif} / F_{\max}^T$, E_a^T, E_a^{dif}, E_a^{dir}. The accuracy of our simple location/time-scaling approach was less viable (see Table 5) than the excellent accuracy of the regression model (see Tables 1–4), but it was still within the general accuracy attained in the virus inactivation studies.

The approach, equations, and procedure presented in this study should assist in estimating the time during which viral and other pathogens remain infectious after accidental or intentional release in the atmosphere. The demonstrated success of the regression model should encourage other researchers to seek simple regression models for complex MODTRAN computations in a variety of additional applications.

Table 1. 1976 U.S. Standard Atmosphere with Rural Aerosols at Latitude 35° at Four Equinox and Solstice Dates

Regression Model: $y(h,alb,vis) = w_1 + w_2 h + w_3 h^2 + w_4 alb + w_5 alb^2 + w_6 vis + w_7 vis^2$

$0 \le h \le 5(km)$ $0 \le albedo \le 0.15$ $15km \le visibility \le 100km$

y	Day	w_1	w_2	w_3	w_4	w_5	w_6	w_7	Mean |error| (%)	Max |error| (%) with $P \ge 0.9$
$\frac{E_a^T}{F_{\max}^T}$	Mar 21	2.61E+01	9.79E-01	-5.20E-02	-1.87E+00	6.60E-02	1.17E-02	-7.08E-05	0.18	0.37
	Jun 21	4.01E+01	1.66E+00	-9.59E-02	-3.36E+00	1.69E-01	1.90E-02	-1.15E-04	0.22	0.47
	Sep 21	2.68E+01	1.03E+00	-5.73E-02	-1.95E+00	7.88E-02	1.18E-02	-7.14E-05	0.19	0.39
	Dec 21	1.14E+01	2.20E-01	-4.26E-03	-4.85E-01	-1.37E-02	2.49E-03	-1.47E-05	0.09	0.20
$\frac{E_a^{dif}}{F_{\max}^{dif}}$	Mar 21	2.77E+01	1.10E+00	-8.48E-02	-7.60E+00	6.66E+00	3.78E-02	-2.21E-04	0.41	0.94
	Jun 21	4.30E+01	1.80E+00	-1.56E-01	-1.44E+01	1.46E+01	5.32E-02	-3.15E-04	0.43	0.94
	Sep 21	2.86E+01	1.15E+00	-9.60E-02	-8.34E+00	7.69E+00	3.88E-02	-2.28E-04	0.43	0.95
	Dec 21	1.18E+01	3.43E-01	-1.64E-02	-1.91E+00	1.22E+00	1.59E-02	-9.00E-05	0.33	0.78
$\frac{F_{\max}^{dir}}{E_a^T}$	Mar 21	8.58E-03	8.38E-04	-2.58E-05	-1.43E-02	9.13E-03	1.52E-04	-8.81E-07	4.57	10.05
	Jun 21	7.32E-03	3.73E-04	-7.43E-06	-1.10E-02	7.12E-03	9.93E-05	-5.82E-07	3.96	9.14
	Sep 21	9.08E-03	8.80E-04	-4.50E-05	-1.47E-02	9.37E-03	1.49E-04	-8.70E-07	4.50	9.81
	Dec 21	7.65E-03	3.42E-03	-1.46E-04	-1.93E-02	1.18E-02	2.83E-04	-1.60E-06	6.38	13.85
$\frac{E_a^T}{E_a^{dif}}$	Mar 21	1.21E+00	6.47E-02	3.87E-03	-7.51E-01	7.28E-01	6.96E-03	-3.81E-05	1.55	3.65
	Jun 21	1.32E+00	7.17E-02	4.66E-03	-1.16E+00	1.28E+00	8.92E-03	-4.89E-05	1.87	4.30
	Sep 21	1.23E+00	7.61E-02	2.48E-03	-8.47E-01	8.46E-01	7.41E-03	-4.09E-05	1.68	3.86
	Dec 21	1.05E+00	4.90E-02	2.11E-03	-2.46E-01	1.79E-01	3.30E-03	-1.79E-05	0.86	2.05
$\frac{E^{dir}}{E_a^T}$	Mar 21	1.34E+02	2.24E+01	-5.75E-01	-2.47E+02	1.56E+02	2.91E+00	-1.67E-02	1.55	3.65
	Jun 21	1.38E+02	1.48E+01	-3.80E-01	-2.28E+02	1.46E+02	2.33E+00	-1.35E-02	1.87	4.30
	Sep 21	1.44E+02	2.41E+01	-1.05E+00	-2.58E+02	1.63E+02	2.90E+00	-1.68E-02	1.68	3.86
	Dec 21	8.42E+01	5.35E+01	-1.45E+00	-2.50E+02	1.50E+02	3.91E+00	-2.18E-02	0.86	2.05
$\frac{F_{\max}^{dif}}{F_{\max}^T}$	Mar 21	7.77E-01	-3.48E-02	9.19E-04	4.14E-01	-2.65E-01	-4.17E-03	2.42E-05	2.45	5.75
	Jun 21	7.08E-01	-3.15E-02	9.04E-04	4.95E-01	-3.22E-01	-4.24E-03	2.48E-05	2.81	6.56
	Sep 21	7.58E-01	-3.77E-02	1.60E-03	4.36E-01	-2.80E-01	-4.20E-03	2.46E-05	2.63	6.17
	Dec 21	9.14E-01	-4.32E-02	1.31E-03	2.35E-01	-1.44E-01	-3.31E-03	1.87E-05	1.58	3.74
E_a^T	Mar 21	5.57E+01	1.76E+01	-9.23E-01	7.12E+01	2.87E+01	1.48E-01	-8.88E-04	1.74	3.58
	Jun 21	1.22E+02	3.47E+01	-1.92E+00	1.53E+02	6.02E+01	2.90E-01	-1.74E-03	1.57	3.24
	Sep 21	5.87E+01	1.84E+01	-1.01E+00	7.45E+01	2.98E+01	1.46E-01	-8.79E-04	1.72	3.54
	Dec 21	9.11E+00	3.29E+00	-1.49E-01	1.20E+01	4.99E+00	2.67E-02	-1.60E-04	1.96	4.00
E_a^{dif}	Mar 21	4.73E+01	1.00E+01	-1.02E+00	7.12E+01	2.87E+01	-1.53E-01	8.16E-04	1.23	2.52
	Jun 21	9.49E+01	1.72E+01	-1.87E+00	1.53E+02	6.02E+01	-4.05E-01	2.24E-03	1.22	2.49
	Sep 21	4.88E+01	9.78E+00	-1.00E+00	7.45E+01	2.98E+01	-1.73E-01	9.42E-04	1.22	2.50
	Dec 21	8.81E+00	2.40E+00	-2.07E-01	1.20E+01	4.99E+00	-5.49E-03	1.65E-05	1.56	3.20
E_a^{dir}	Mar 21	8.36E+00	7.60E+00	1.02E-01	-2.51E-13	1.46E-12	3.01E-01	-1.70E-03	4.82	10.26
	Jun 21	2.67E+01	1.75E+01	-5.39E-02	-6.76E-13	3.75E-12	6.95E-01	-3.98E-03	4.32	9.37
	Sep 21	9.90E+00	8.65E+00	-1.09E-02	-1.85E-13	1.05E-12	3.18E-01	-1.82E-03	4.89	10.31
	Dec 21	3.04E-01	8.95E-01	5.74E-02	-3.53E-14	1.92E-13	3.22E-02	-1.76E-04	6.37	15.25

Altitude h and visibility vis are in kilometers. Albedo alb is in fractions (0–1).This is a rural aerosol model (MODTRAN parameter *ihaze*). 21 March and 21 June are with the spring-summer seasonal model (MODTRAN parameter *iseasn*); 21 September and 21 December are with fall-winter seasonal model. The mean absolute error in the regression model and the maximum absolute error (for probability >0.9) were computed for 1760 values h, alb, and vis. The Table shows excellent fit of the regression model to the complex MODTRAN radiation fields and 2.1% mean error (for all 36 entries). The worst accuracy (~6%) is for radiation fields E_a^{dir} and $F_{\max}^{dir} / E_a^T$ at 21 December. For all other radiation fields, the mean absolute error is less than 5% (for most entries the error is <2%, mean of 1.85% for all other 34 entries).

Table 2. 1976 U.S. Standard Atmosphere with Urban Aerosols at Latitude 35° at Four Equinox and Solstice Dates

Regression Model: $y(h,alb,vis) = w_1 + w_2 h + w_3 h^2 + w_4 alb + w_5 alb^2 + w_6 vis + w_7 vis^2$

$0 \le h \le 5(km)$ $0 \le albedo \le 0.15$ $15km \le visibility \le 100km$

y	Day	w_1	w_2	w_3	w_4	w_5	w_6	w_7	Mean |error| (%)	Max |error| (%) with $P \ge 0.9$
$\frac{E_a^T}{F_{max}^T}$	Mar 21	2.60E+01	1.03E+00	-5.51E-02	-1.62E+00	1.49E-01	1.27E-02	-7.72E-05	0.25	0.57
	Jun 21	3.98E+01	1.74E+00	-1.01E-01	-2.90E+00	3.04E-01	2.27E-02	-1.39E-04	0.30	0.70
	Sep 21	2.67E+01	1.08E+00	-6.05E-02	-1.68E+00	1.63E-01	1.32E-02	-8.06E-05	0.26	0.60
	Dec 21	1.15E+01	2.25E-01	-4.17E-03	-4.13E-01	1.46E-02	1.21E-04	-3.34E-08	0.08	0.16
$\frac{E_a^{dif}}{F_{max}^{dif}}$	Mar 21	2.83E+01	1.11E+00	-8.21E-02	-7.57E+00	7.07E+00	2.73E-02	-1.62E-04	0.48	1.10
	Jun 21	4.37E+01	1.84E+00	-1.53E-01	-1.43E+01	1.53E+01	3.92E-02	-2.37E-04	0.50	1.16
	Sep 21	2.92E+01	1.17E+00	-9.34E-02	-8.35E+00	8.18E+00	2.76E-02	-1.66E-04	0.50	1.14
	Dec 21	1.22E+01	3.37E-01	-1.51E-02	-1.90E+00	1.32E+00	9.68E-03	-5.50E-05	0.34	0.78
$\frac{F_{max}^{dir}}{E_a^T}$	Mar 21	1.16E-02	4.90E-04	7.72E-06	-1.44E-02	9.30E-03	9.81E-05	-5.71E-07	3.27	7.21
	Jun 21	9.47E-03	1.07E-04	1.95E-05	-1.10E-02	7.20E-03	5.93E-05	-3.46E-07	2.73	6.31
	Sep 21	1.22E-02	5.21E-04	-1.03E-05	-1.48E-02	9.55E-03	9.26E-05	-5.45E-07	3.19	7.15
	Dec 21	1.16E-02	3.11E-03	-1.28E-04	-1.96E-02	1.22E-02	2.20E-04	-1.27E-06	5.20	11.18
$\frac{E_a^T}{E_a^{dif}}$	Mar 21	1.32E+00	5.63E-02	4.71E-03	-7.97E-01	7.91E-01	5.23E-03	-2.91E-05	1.48	3.37
	Jun 21	1.48E+00	5.80E-02	6.10E-03	-1.25E+00	1.40E+00	6.47E-03	-3.60E-05	1.74	3.90
	Sep 21	1.36E+00	6.73E-02	3.30E-03	-9.04E-01	9.25E-01	5.42E-03	-3.05E-05	1.60	3.57
	Dec 21	1.09E+00	4.84E-02	2.12E-03	-2.54E-01	1.89E-01	2.72E-03	-1.51E-05	0.92	2.16
$\frac{E^{dir}}{E_a^T}$	Mar 21	1.83E+02	1.70E+01	-8.29E-02	-2.49E+02	1.59E+02	2.05E+00	-1.18E-02	1.48	3.37
	Jun 21	1.81E+02	9.79E+00	1.08E-01	-2.29E+02	1.48E+02	1.55E+00	-8.99E-03	1.74	3.90
	Sep 21	1.96E+02	1.84E+01	-5.39E-01	-2.60E+02	1.66E+02	1.98E+00	-1.16E-02	1.60	3.57
	Dec 21	1.32E+02	5.04E+01	-1.32E+00	-2.53E+02	1.55E+02	3.16E+00	-1.80E-02	0.92	2.16
$\frac{F_{max}^{dif}}{F_{max}^T}$	Mar 21	7.00E-01	-2.71E-02	1.76E-04	4.14E-01	-2.67E-01	-2.76E-03	1.60E-05	2.12	4.86
	Jun 21	6.22E-01	-2.26E-02	-7.66E-06	4.91E-01	-3.22E-01	-2.63E-03	1.54E-05	2.35	5.38
	Sep 21	6.75E-01	-2.96E-02	8.23E-04	4.36E-01	-2.82E-01	-2.68E-03	1.58E-05	2.27	5.24
	Dec 21	8.67E-01	-4.02E-02	1.12E-03	2.38E-01	-1.48E-01	-2.55E-03	1.47E-05	1.54	3.61
E_a^T	Mar 21	4.09E+01	1.81E+01	-9.02E-01	6.21E+01	2.09E+01	4.66E-01	-2.80E-03	2.46	4.81
	Jun 21	9.25E+01	3.59E+01	-1.93E+00	1.34E+02	4.42E+01	9.18E-01	-5.54E-03	2.26	4.37
	Sep 21	4.33E+01	1.90E+01	-9.96E-01	6.50E+01	2.17E+01	4.78E-01	-2.88E-03	2.43	4.73
	Dec 21	6.33E+00	3.34E+00	-1.40E-01	1.03E+01	3.58E+00	8.60E-02	-5.13E-04	2.69	5.29
E_a^{dif}	Mar 21	3.20E+01	1.07E+01	-1.02E+00	6.21E+01	2.09E+01	1.72E-01	-1.13E-03	1.89	3.73
	Jun 21	6.46E+01	1.88E+01	-1.92E+00	1.34E+02	4.42E+01	2.42E-01	-1.65E-03	1.72	3.52
	Sep 21	3.28E+01	1.05E+01	-1.01E+00	6.50E+01	2.17E+01	1.68E-01	-1.10E-03	1.82	3.55
	Dec 21	5.97E+00	2.46E+00	-1.99E-01	1.03E+01	3.58E+00	5.43E-02	-3.39E-04	2.33	4.55
E_a^{dir}	Mar 21	8.87E+00	7.45E+00	1.19E-01	-2.40E-13	1.42E-12	2.94E-01	-1.67E-03	4.58	9.90
	Jun 21	2.79E+01	1.71E+01	-1.01E-02	-4.93E-13	2.95E-12	6.76E-01	-3.88E-03	4.11	8.91
	Sep 21	1.05E+01	8.49E+00	8.95E-03	-2.69E-13	1.36E-12	3.10E-01	-1.78E-03	4.64	9.96
	Dec 21	3.52E-01	8.81E-01	5.89E-02	-1.46E-14	1.05E-13	3.17E-02	-1.75E-04	6.03	14.56

Same as Table 1, but for 1976 U.S. standard atmosphere with urban aerosols. The Table shows excellent fit of the regression model and 2% mean error (all 36 entries). The worst accuracy (~6%) is for radiation fields E_a^{dir} and F_{max}^{dir} / E_a^T at 21 December. For all other radiation fields, the mean absolute error <5% (mean of 1.84% for all other 34 entries).

Table 3. Mid-Latitude Atmosphere with Rural Aerosols at Latitude 35° at Four Equinox and Solstice Dates

Regression Model: $y(h,alb,vis) = w_1 + w_2 h + w_3 h^2 + w_4 alb + w_5 alb^2 + w_6 vis + w_7 vis^2$

$0 \le h \le 5(km)$ $0 \le albedo \le 0.15$ $15km \le visibility \le 100km$

y	Day	w_1	w_2	w_3	w_4	w_5	w_6	w_7	Mean |error| (%)	Max |error| (%) with $P \ge 0.9$
$\frac{E_a^T}{F_{\max}^T}$	Mar 21	2.69E+01	1.01E+00	-4.04E-02	-2.21E+00	3.51E-02	1.27E-02	-7.62E-05	0.19	0.38
	Jun. 21	4.14E+01	1.70E+00	-7.65E-02	-3.94E+00	1.31E-01	2.03E-02	-1.23E-04	0.23	0.47
	Sep 21	2.33E+01	8.62E-01	-5.25E-02	-1.61E+00	6.65E-02	9.47E-03	-5.74E-05	0.19	0.38
	Dec 21	1.01E+01	1.79E-01	-4.13E-03	-4.02E-01	-1.33E-02	1.99E-03	-1.18E-05	0.09	0.19
$\frac{E_a^{dif}}{F_{\max}^{dif}}$	Mar 21	2.86E+01	1.11E+00	-7.91E-02	-8.09E+00	6.85E+00	3.79E-02	-2.22E-04	0.40	0.88
	Jun 21	4.43E+01	1.79E+00	-1.47E-01	-1.52E+01	1.49E+01	5.17E-02	-3.07E-04	0.41	0.88
	Sep 21	2.48E+01	9.69E-01	-8.98E-02	-6.98E+00	6.47E+00	3.20E-02	-1.88E-04	0.42	0.94
	Dec 21	1.05E+01	2.93E-01	-1.51E-02	-1.66E+00	1.07E+00	1.40E-02	-7.88E-05	0.34	0.78
$\frac{F_{\max}^{dir}}{E_a^T}$	Mar. 21	8.32E-03	8.27E-04	-3.56E-05	-1.37E-02	8.77E-03	1.48E-04	-8.57E-07	4.61	10.21
	Jun. 21	7.10E-03	3.75E-04	-1.51E-05	-1.05E-02	6.83E-03	9.67E-05	-5.67E-07	4.00	9.28
	Sep 21	1.05E-02	1.09E-03	-5.07E-05	-1.70E-02	1.08E-02	1.73E-04	-1.02E-06	4.53	9.80
	Dec 21	8.63E-03	4.04E-03	-1.65E-04	-2.19E-02	1.33E-02	3.23E-04	-1.83E-06	6.38	13.83
$\frac{E_a^T}{E_a^{dif}}$	Mar 21	1.21E+00	6.69E-02	3.96E-03	-7.61E-01	7.40E-01	7.13E-03	-3.90E-05	1.58	3.71
	Jun 21	1.32E+00	7.54E-02	4.80E-03	-1.19E+00	1.31E+00	9.20E-03	-5.04E-05	1.91	4.39
	Sep 21	1.24E+00	7.90E-02	3.23E-03	-8.70E-01	8.70E-01	7.59E-03	-4.19E-05	1.70	3.90
	Dec 21	1.05E+00	5.04E-02	2.35E-03	-2.48E-01	1.80E-01	3.33E-03	-1.81E-05	0.86	2.06
$\frac{E^{dir}}{E_a^T}$	Mar 21	1.30E+02	2.19E+01	-7.66E-01	-2.37E+02	1.50E+02	2.83E+00	-1.63E-02	1.58	3.71
	Jun 21	1.34E+02	1.46E+01	-5.51E-01	-2.18E+02	1.40E+02	2.27E+00	-1.32E-02	1.91	4.39
	Sep 21	1.66E+02	2.91E+01	-1.18E+00	-2.97E+02	1.87E+02	3.37E+00	-1.95E-02	1.70	3.90
	Dec 21	9.47E+01	6.26E+01	-1.57E+00	-2.83E+02	1.69E+02	4.43E+00	-2.48E-02	0.86	2.06
$\frac{F_{\max}^{dif}}{F_{\max}^T}$	Mar 21	7.77E-01	-3.52E-02	1.03E-03	4.14E-01	-2.66E-01	-4.20E-03	2.43E-05	2.47	5.80
	Jun 21	7.07E-01	-3.21E-02	1.03E-03	4.95E-01	-3.23E-01	-4.26E-03	2.49E-05	2.84	6.64
	Sep 21	7.57E-01	-3.91E-02	1.61E-03	4.37E-01	-2.79E-01	-4.24E-03	2.48E-05	2.70	6.31
	Dec 21	9.14E-01	-4.47E-02	1.32E-03	2.36E-01	-1.43E-01	-3.34E-03	1.89E-05	1.61	3.79
E_a^T	Mar 21	5.82E+01	1.79E+01	-8.45E-01	7.33E+01	2.83E+01	1.52E-01	-9.12E-04	1.72	3.54
	Jun 21	1.27E+02	3.52E+01	-1.76E+00	1.57E+02	5.90E+01	2.97E-01	-1.78E-03	1.55	3.21
	Sep 21	4.79E+01	1.51E+01	-8.86E-01	6.03E+01	2.41E+01	1.11E-01	-6.65E-04	1.65	3.39
	Dec 21	7.44E+00	2.71E+00	-1.31E-01	9.69E+00	4.03E+00	2.05E-02	-1.22E-04	1.87	3.87
E_a^{dif}	Mar 21	4.93E+01	1.01E+01	-9.94E-01	7.33E+01	2.83E+01	-1.65E-01	8.86E-04	1.22	2.51
	Jun 21	9.87E+01	1.70E+01	-1.80E+00	1.57E+02	5.90E+01	-4.36E-01	2.42E-03	1.25	2.56
	Sep 21	3.97E+01	7.89E+00	-8.65E-01	6.03E+01	2.41E+01	-1.50E-01	8.26E-04	1.24	2.54
	Dec 21	7.19E+00	1.96E+00	-1.78E-01	9.69E+00	4.03E+00	-5.79E-03	2.19E-05	1.50	3.08
E_a^{dir}	Mar 21	8.85E+00	7.89E+00	1.49E-01	-2.33E-13	1.33E-12	3.18E-01	-1.80E-03	4.81	10.36
	Jun 21	2.82E+01	1.82E+01	4.37E-02	-7.13E-13	3.82E-12	7.34E-01	-4.21E-03	4.31	9.40
	Sep 21	8.13E+00	7.23E+00	-2.08E-02	-2.76E-13	1.38E-12	2.60E-01	-1.49E-03	4.84	10.27
	Dec 21	2.47E-01	7.48E-01	4.64E-02	-1.08E-14	5.29E-14	2.62E-02	-1.44E-04	6.28	14.99

Same as Table 1 but for mid-latitude atmosphere with rural aerosols. 21 March and 21 June are for mid-latitude-summer atmosphere at spring-summer season model. 21 September and 21 December are for mid-latitude-winter atmosphere at spring-summer season. The Table shows excellent fit of the regression model and 2.1% mean error (considering all 36 entries). The worst accuracy (~6%) is for radiation fields E_a^{dir} and $F_{\max}^{dir} / E_a^T$ at 21 December. For all other radiation fields, the mean absolute error is <5% (a mean of 1.85% for all other 34 entries).

Table 4. Mid-Latitude Atmosphere with Urban Aerosols at Latitude 35° at Four Equinox and Solstice Dates

Regression Model: $y(h,alb,vis) = w_1 + w_2 h + w_3 h^2 + w_4 alb + w_5 alb^2 + w_6 vis + w_7 vis^2$

$0 \le h \le 5(km)$ $0 \le albedo \le 0.15$ $15km \le visibility \le 100km$

y	Day	w_1	w_2	w_3	w_4	w_5	w_6	w_7	Mean $\lvert error \rvert$ (%)	Max $\lvert error \rvert$ (%) with $P \ge 0.9$
$\frac{E_a^T}{F_{max}^T}$	Mar 21	2.69E+01	1.06E+00	-4.30E-02	-1.93E+00	1.32E-01	1.20E-02	-7.30E-05	0.24	0.55
	Jun 21	4.13E+1	1.78E+0	-8.06E-2	-3.43E+0	2.88E-1	2.13E-2	-1.31E-4	0.29	0.67
	Sep 21	2.33E+01	8.62E-01	-5.25E-02	-1.61E+00	6.65E-02	9.47E-03	-5.74E-05	0.19	0.38
	Dec 21	1.02E+01	1.82E-01	-4.02E-03	-3.49E-01	8.83E-03	1.53E-04	-3.34E-07	0.08	0.16
$\frac{E_a^{dif}}{F_{max}^{dif}}$	Mar 21	2.92E+01	1.12E+00	-7.67E-02	-8.01E+00	7.24E+00	2.63E-02	-1.57E-04	0.46	1.07
	Jun 21	4.51E+01	1.83E+00	-1.43E-01	-1.50E+01	1.56E+01	3.58E-02	-2.19E-04	0.48	1.11
	Sep 21	2.48E+01	9.69E-01	-8.98E-02	-6.98E+00	6.47E+00	3.20E-02	-1.88E-04	0.42	0.94
	Dec 21	1.07E+01	2.90E-01	-1.43E-02	-1.66E+00	1.15E+00	9.15E-03	-5.19E-05	0.35	0.80
$\frac{F_{max}^{dir}}{E_a^T}$	Mar 21	1.09E-02	5.27E-04	-7.79E-06	-1.38E-02	8.93E-03	1.01E-04	-5.86E-07	3.43	7.59
	Jun 21	8.99E-03	1.45E-04	7.54E-06	-1.06E-02	6.91E-03	6.16E-05	-3.60E-07	2.87	6.59
	Sep 21	1.05E-02	1.09E-03	-5.07E-05	-1.70E-02	1.08E-02	1.73E-04	-1.02E-06	4.53	9.80
	Dec 21	1.25E-02	3.78E-03	-1.53E-04	-2.22E-02	1.37E-02	2.60E-04	-1.50E-06	5.40	11.63
$\frac{E_a^T}{E_a^{dif}}$	Mar 21	1.32E+00	5.98E-02	4.62E-03	-8.04E-01	7.99E-01	5.55E-03	-3.08E-05	1.53	3.48
	Jun 21	1.47E+00	6.35E-02	5.97E-03	-1.26E+00	1.43E+00	6.96E-03	-3.87E-05	1.80	4.04
	Sep 21	1.24E+00	7.90E-02	3.23E-03	-8.70E-01	8.70E-01	7.59E-03	-4.19E-05	1.70	3.90
	Dec 21	1.09E+00	5.04E-02	2.30E-03	-2.55E-01	1.89E-01	2.81E-03	-1.56E-05	0.94	2.20
$\frac{E^{dir}}{E_a^T}$	Mar 21	1.73E+02	1.73E+01	-3.62E-01	-2.39E+02	1.53E+02	2.08E+00	-1.20E-02	1.53	3.48
	Jun 21	1.72E+02	1.03E+01	-1.43E-01	-2.19E+02	1.42E+02	1.59E+00	-9.20E-03	1.80	4.04
	Sep 21	1.66E+02	2.91E+01	-1.18E+00	-2.97E+02	1.87E+02	3.37E+00	-1.95E-02	1.70	3.90
	Dec 21	1.42E+02	6.02E+01	-1.54E+00	-2.86E+02	1.74E+02	3.70E+00	-2.10E-02	0.94	2.20
$\frac{F_{max}^{dif}}{F_{max}^T}$	Mar 21	7.06E-01	-2.84E-02	4.03E-04	4.14E-01	-2.68E-01	-2.90E-03	1.69E-05	2.19	5.04
	Jun 21	6.28E-01	-2.41E-02	2.44E-04	4.92E-01	-3.23E-01	-2.79E-03	1.63E-05	2.44	5.56
	Sep 21	7.57E-01	-3.91E-02	1.61E-03	4.37E-01	-2.79E-01	-4.24E-03	2.48E-05	2.70	6.31
	Dec 21	8.72E-01	-4.24E-02	1.23E-03	2.38E-01	-1.47E-01	-2.67E-03	1.53E-05	1.60	3.74
E_a^T	Mar 21	4.40E+01	1.84E+01	-8.20E-01	6.46E+01	2.10E+01	4.60E-01	-2.76E-03	2.36	4.65
	Jun. 21	9.91E+01	3.63E+01	-1.75E+00	1.39E+02	4.42E+01	9.02E-01	-5.44E-03	2.17	4.26
	Sep 21	4.79E+01	1.51E+01	-8.86E-01	6.03E+01	2.41E+01	1.11E-01	-6.65E-04	1.65	3.39
	Dec 21	5.39E+00	2.73E+00	-1.22E-01	8.47E+00	3.00E+00	6.44E-02	-3.85E-04	2.48	4.90
E_a^{dif}	Mar 21	3.46E+01	1.06E+01	-9.87E-01	6.46E+01	2.10E+01	1.49E-01	-1.00E-03	1.77	3.45
	Jun 21	6.96E+01	1.85E+01	-1.84E+00	1.39E+02	4.42E+01	1.86E-01	-1.34E-03	1.61	3.40
	Sep 21	3.97E+01	7.89E+00	-8.65E-01	6.03E+01	2.41E+01	-1.50E-01	8.26E-04	1.24	2.54
	Dec 21	5.11E+00	1.99E+00	-1.70E-01	8.47E+00	3.00E+00	3.85E-02	-2.42E-04	2.11	4.12
E_a^{dir}	Mar 21	9.35E+00	7.75E+00	1.67E-01	-3.22E-13	1.90E-12	3.11E-01	-1.76E-03	4.58	9.79
	Jun 21	2.94E+01	1.78E+01	8.64E-02	-4.81E-13	2.74E-12	7.16E-01	-4.11E-03	4.11	9.03
	Sep 21	8.13E+00	7.23E+00	-2.08E-02	-2.76E-13	1.38E-12	2.60E-01	-1.49E-03	4.84	10.27
	Dec 21	2.81E-01	7.38E-01	4.75E-02	-1.80E-14	5.71E-14	2.59E-02	-1.43E-04	5.98	14.20

Same as Table 3, but for mid-latitude atmosphere with urban aerosols. The Table shows excellent fit of the regression model and 2.1% mean error (all 36 entries). The worst accuracy (~6%), is for radiation fields E_a^{dir} and F_{max}^{dir} / E_a^T at 21 December. For all other radiation fields, the mean absolute error is <5% (mean of 1.86% for all 34 entries).

Table 5. Mean |*error*| for Latitude/Date Scaling of a Reference Atmosphere to Four Dates and Four Atmospheres

Location and time scaling for regression model $y(latitude = 35^o, Mar.21^{st}) \rightarrow y(latitude, day)$ for atmospheres A, B, C, and D													
Day of Year		Latitude 25 Mean |*error*| (%)				Latitude 35 Mean |*error*| (%)				Latitude 45 Mean |*error*| (%)			
		A	B	C	D	A	B	C	D	A	B	C	D
Feb 1	$E_a^T / F_{\max}^T$	3.0	3.0	18.5	18.6	2.0	2.2	13.7	13.6	15.9	16.4	2.2	2.4
	$E_a^{dif} / F_{\max}^{dif}$	2.9	2.8	18.2	18.2	1.8	2.0	13.5	13.4	14.4	14.7	1.1	1.1
	$F_{\max}^{dif} / F_{\max}^T$	2.8	3.0	2.5	2.8	1.6	1.2	1.7	1.3	8.5	6.4	8.5	6.6
	E_a^T	1.5	1.8	23.4	23.5	12.2	12.9	31.7	32.1	24.0	24.9	40.3	40.9
	E_a^{dif}	2.0	1.9	20.6	20.5	2.4	2.3	22.0	21.6	5.3	4.6	23.5	22.8
	E_a^{dir}	2.5	2.4	21.8	21.8	18.8	18.6	36.9	36.8	46.5	46.2	58.3	58.2
May 1	$E_a^T / F_{\max}^T$	0.9	1.0	0.9	1.0	3.7	3.6	3.7	3.6	10.7	10.6	10.7	10.6
	$E_a^{dif} / F_{\max}^{dif}$	0.9	1.0	1.2	1.3	3.7	3.7	3.6	3.5	10.8	10.7	10.7	10.7
	$F_{\max}^{dif} / F_{\max}^T$	1.0	1.0	1.0	1.0	5.2	5.7	5.3	5.8	12.5	12.7	12.6	12.7
	E_a^T	8.2	9.0	8.1	8.8	4.3	4.8	4.2	4.7	2.1	2.0	2.2	2.0
	E_a^{dif}	2.8	2.9	3.2	3.3	3.5	3.6	3.9	3.9	5.0	5.1	5.2	5.2
	E_a^{dir}	10.8	10.6	10.9	10.7	6.8	6.7	6.8	6.7	1.7	1.7	1.7	1.7
Aug 1	$E_a^T / F_{\max}^T$	0.3	0.3	0.3	0.3	5.1	5.1	5.1	5.1	12.3	12.3	12.3	12.3
	$E_a^{dif} / F_{\max}^{dif}$	0.3	0.3	0.3	0.2	5.2	5.1	5.0	4.9	12.5	12.4	12.3	12.3
	$F_{\max}^{dif} / F_{\max}^T$	1.4	2.0	1.5	2.0	6.9	7.5	7.0	7.5	14.5	14.8	14.5	14.8
	E_a^T	7.0	7.8	6.8	7.6	3.5	4.1	3.4	4.0	2.4	2.1	2.4	2.2
	E_a^{dif}	4.3	4.4	4.8	4.9	5.3	5.4	5.7	5.8	7.0	7.0	7.2	7.2
	E_a^{dir}	9.9	9.7	9.9	9.8	6.6	6.5	6.6	6.5	2.3	2.2	2.2	2.2
Nov 1	$E_a^T / F_{\max}^T$	3.1	3.1	18.7	18.7	1.4	1.5	14.4	14.4	12.4	12.7	3.8	3.6
	$E_a^{dif} / F_{\max}^{dif}$	3.0	2.9	18.3	18.4	1.3	1.5	14.2	14.2	11.4	11.7	4.2	4.1
	$F_{\max}^{dif} / F_{\max}^T$	2.9	2.9	2.6	2.7	1.3	0.9	1.4	1.1	7.7	6.0	7.8	6.1
	E_a^T	0.3	0.4	22.1	22.1	9.8	10.4	29.9	30.2	21.5	22.4	38.7	39.2
	E_a^{dif}	1.0	0.8	21.4	21.3	1.9	1.8	22.5	22.3	4.9	4.4	24.3	23.6
	E_a^{dir}	3.8	3.8	19.2	19.2	13.1	12.9	32.3	32.2	37.8	37.5	51.6	51.5

Each of the six quantities are scaled (eq 16) from a reference atmosphere at a reference date and latitude to four atmospheres (A, B, C, and D) at four dates (1 February, 1 May, 1 August, and 1 November) and three latitudes (25, 35, and 45°). The error is computed over all parameter spaces $(h, albedo, visibility)$. Atmosphere A is U.S. 1976 standard with rural aerosols. Atmosphere B is U.S. 1976 standard with urban aerosols. Atmosphere C is mid-latitude-summer atmosphere with rural aerosols. Atmosphere D is mid-latitude-summer atmosphere with urban aerosols. 1 February and 1 November are fall-winter season. 1 May and 1 August are spring-summer season. Reference atmosphere is same as in A, B, C, and D atmospheres at spring-summer. The reference date and location are 21 March at latitude 35°. Average of all 288 entries is ~10%, where the error is $\leq 5\%$ for 130 entries.

LITERATURE CITED

1. Ben-David, A.; Sagripanti, J. L. A model for inactivation of microbes suspended in the atmosphere by solar ultraviolet radiation. *Photochem. Photobiol.* **2010,** *86*, 895–908.

2. Berk, A.; Anderson, G. P.; Acharya, P. K.; Bernstein, L. S.; Muratov, L.; Lee, J.; Fox, M.; Adler-Golden, S. M.; Chetwynd, J. H.; Hoke, M. L.; Lockwood, R. B.; Cooley, T. W.; Gardner, J. A. MODTRAN5: A reformulated atmospheric band model with auxiliary species and practical multiple scattering options. *Proc. SPIE Int. Soc. Opt. Eng.* **2005**, *5655*, 88–95.

3. Jagger, J. *Solar-UV Actions on Living Cells*; Praeger: Westport, CT, 1985.

4. U.S. Air Force. MODTRAN4 - MODerate spectral resolution atmospheric TRANsmittance algorithm and computer model, developed by AFRL/VSBT in collaboration with Spectral Sciences. http://www.kirtland.af.mil/library/factsheets/factsheet.asp?id=7915 (accessed Sep 2011).

5. Ontar Corporation home page. www.ontar.com (accessed Sep 2011).

6. Patterson, E. M.; Gillespie, J. B. Simplified ultaviolet and visible wavelength atmospheric propagation model. *Appl. Opt.* **1989**, *28*, 425–429.

7. Tornow, C.; Borel, C. C.; Powers, B. J. Robust temperature retrieval using multi-spectral and multi-angular IR measurements. *Proceedings of IGARSS'1994*, Pasadena, CA, June 6–8, 1994; 441–443.

8. Asmat, A.; Milton, E. J.; Atkinson, P. M. Atmospheric correction of multiple flightline hyperspectral data (CASI-2). *Proceedings of the Remote Sensing and Photogrammetry Society Conference*, University of Exeter, UK, September 15–17, 2008.

9. Liou, K. N. *An Introduction to Atmospheric Radiation*; 2nd ed.; Academic Press: London, UK, 2002.

10. Berk., A.; Anderson, G. P.; Acharya, P. K.; Bernstein, L. S.; Chetwynd, J. H.; Matthew, M. W.; Shettle, E. P.; Adler-Golden, S. M. MODTRAN4 User's Manual; U.S. Air Force Research Laboratory Report, Wright Patterson Air Force Base, OH, 1999.

11. Lytle, C. D.; Sagripanti, J.-L. Predicted inactivation of viruses of relevance to biodefense. *J. Virolol.* **2005**, *79*, 14244–14252.

12. Jagger, J. *Introduction to Research in Ultraviolet Photobiology*; Prentice-Hall, Inc.: Upper Saddle River, NJ, 1967.

13. National Oceanic and Atmospheric Administration home page, solar angle equation. http://www.srrb.noaa.gov/highlights/sunrise/solareqns.PDF (accessed Sep 2011).

14. Koschmieder, H. Theorie der horizontalen Sichtweite. *Beit. Phys. Atmos.* **1926**, *12*, 33–55.

15. Griffing, G. W. Relations between the prevailing visibility, nephelometer scattering coefficient and sunphotometer turbidity coefficient. *Atmos. Environ.* **1980**, *14*, 577–584.

16. Husar, R. B.; Husar, J. D.; Martin, L. Distribution of continental surface aerosol extinction based on visual range data. *Atmos. Environ.* **2000**, *34*, 5067–5078.

17. Fiester, U.; Grewe, R. Spectral albedo measurements in the UV and visible region over different types of surfaces. *Photochem. Photobiol.* **1995,** *62*, 736–744.

18. Golub, G. H.; Van Loan, C. F. *Matrix Computations*, 3rd ed.; The Johns Hopkins University Press: Baltimore, MD, 1996.

19. Twomey, S. *Introduction to the Mathematics of Inversion in Remote Sensing and Indirect Measurements*; Dover Publications, Inc.: Mineola, NY, 1977.

20. World Health Organization. World population by sub-regions at 10 degree bands of latitude. http://www.who.int/uv/health/solaruvradann4_6.pdf (accessed Sep 2011).

21. Adler-Golden, M.; Matthew, M. W.; Bernstein, L. S.; Levine, R. Y.; Berk, A.; Richtsmeier, S. C.; Acharya, P. K.; Anderson, G. P.; Felde, G.; Gardner, J.; Hoke, M.; Jeong, L. S.; Pukall, B.; Mello, J.; Ratkowski, A.; Burke, H.-H. Atmospheric correction for short-wave spectral imagery based on MODTRAN4. *SPIE Proceeding, Imaging Spectrometry V.* **1999**, *3753*, 61–69.

22. Smith, W. J. *Modern Optical Engineering, The Design of Optical Systems*; 2nd ed.; McGraw-Hill: Columbus, OH, 1990.